Check for updates

Chemistry – A European Journal

ChemEurJ Chemistry Europe European Chemical Societies Publishing

RESEARCH ARTICLE OPEN ACCESS

Countercation Manipulation Enables Selective Electrochemical CO_2-to-Formate Conversion Over Bi-Polyoxometalate-Derived Catalysts

Kimitake Kawakami[1] | Kentaro Yonesato[1,2] | Shimon Akino[1] | Soichi Kikkawa[3] | Seiji Yamazoe[3] | Takuma Kaneko[4] | Tomoya Uruga[4] | Fumiaki Amano[5] | Yoshiaki Honjo[6] | Takaki Hatsui[6] | Koji Harano[7,8] | Kazuya Yamaguchi[1] | Kosuke Suzuki[1,2]

[1]Department of Applied Chemistry, School of Engineering, The University of Tokyo, Tokyo, Japan | [2]Department of Advanced Materials Science, Graduate School of Frontier Sciences, The University of Tokyo, Kashiwa-shi, Chiba, Japan | [3]Department of Chemistry, Graduate School of Science, Tokyo Metropolitan University, Tokyo, Japan | [4]Japan Synchrotron Radiation Research Institute (JASRI), Hyogo, Japan | [5]Department of Applied Chemistry for Environment, Graduate School of Urban Environmental Sciences, Tokyo Metropolitan University, Tokyo, Japan | [6]RIKEN SPring-8 Center, Hyogo, Japan | [7]Center for Basic Research on Materials, National Institute for Materials Science (NIMS), Tsukuba-shi, Ibaraki, Japan | [8]Research Center for Autonomous Systems Materialogy (ASMat), Institute of Integrated Research, Institute of Science Tokyo, Yokohama-shi, Kanagawa, Japan

Correspondence: Kosuke Suzuki (ksuzuki@appchem.t.u-tokyo.ac.jp)

Received: 18 February 2026 | **Revised:** 29 June 2026 | **Accepted:** 3 July 2026

Keywords: bismuth | electrochemical CO_2 reduction reaction | electrode catalysts | nanocatalysts | polyoxometalates

ABSTRACT

Electrochemical conversion of CO_2 into formate ($HCOO^-$) represents a promising strategy for mitigating global warming while producing an industrially important chemical. Polyoxometalates (POMs), anionic molecular metal-oxo clusters, offer unique opportunities as catalysts and catalyst precursors for the electrochemical CO_2 reduction reaction (CO_2RR) owing to their structural diversity, compositional tunability, and flexibility in countercation selection. Despite these advantages, effective strategies for developing POM-based CO_2RR catalysts with high selectivity toward $HCOO^-$ remain limited. In this study, we demonstrate countercation manipulation as a powerful approach to achieving selective $HCOO^-$ production using a bismuth (Bi)-incorporated POM, $[Bi_4O(\gamma\text{-}SiW_{10}O_{36})_2(OAc)]^{7-}$ (**Bi4**). Under gas-diffusion CO_2RR conditions with a 2 M $KHCO_3$ aqueous electrolyte, the Ba^{2+} salt of **Bi4** immobilized on carbon (Ba-**Bi4**/C) exhibited high $HCOO^-$ selectivity with a Faradaic efficiency of 84.3% at −0.79 V_{RHE}, whereas the corresponding tetra-*n*-butylammonium (TBA^+) salt (TBA-**Bi4**/C) exhibited substantially lower selectivity (26.6% at −0.79 V_{RHE}). Post-reaction analyses revealed that both catalysts transformed into highly dispersed Bi species protected by WO_x nanoaggregates. Control experiments and detailed characterizations indicated that the countercations, in conjunction with the POM-derived catalyst structure, play a crucial role in governing CO_2RR performance.

1 | Introduction

Recent global warming, caused primarily by anthropogenic emissions of carbon dioxide (CO_2), poses a serious threat to modern society [1]. To mitigate this climate crisis, considerable efforts have been devoted to developing technologies that utilize CO_2 as a chemical feedstock. Among the various CO_2 utilization strategies, electrochemical CO_2 reduction reaction (CO_2RR) is particularly attractive because it enables the conversion of CO_2 into value-added chemicals and fuels under mild conditions using renewable electricity [2, 3]. Among the possible CO_2RR products, formic acid (HCOOH) and its conjugate base,

This is an open access article under the terms of the Creative Commons Attribution License, which permits use, distribution and reproduction in any medium, provided the original work is properly cited.
© 2026 The Author(s). *Chemistry - A European Journal* published by Wiley-VCH GmbH.

formate ($HCOO^-$), are especially appealing. HCOOH is an important industrial chemical widely used in agriculture, leather processing, food preservation, and pharmaceutical industries [4], and has recently attracted attention as a promising hydrogen carrier owing to its high stability, low toxicity, low flammability, and moderate volumetric energy density. Notably, the decomposition of HCOOH/$HCOO^-$ produces only CO_2 as a by-product, enabling a closed carbon cycle in which CO_2 can be recycled to regenerate HCOOH—a feature that is often difficult to achieve with other hydrogen carriers [5]. In addition, techno-economic analyses suggest that CO_2RR-based production of HCOOH is considered economically viable [6]. Therefore, the development of efficient CO_2RR systems for HCOOH/$HCOO^-$ production is highly desirable.

The catalytic performance of CO_2RR is strongly governed by both the catalyst material and the electrolyte composition. Among various metals, bismuth (Bi)-based catalysts are known to exhibit high selectivity toward $HCOO^-$ while effectively suppressing the competing hydrogen (H_2) evolution reaction owing to their high overpotential for H_2 production [7, 8]. In parallel, the identity of electrolyte cations plays a crucial role in determining CO_2RR activity and selectivity. Larger alkali metal cations, such as Cs^+ and K^+, have been reported to enhance CO_2RR performance by modulating the interfacial electric field, local pH, and stabilization of key reaction intermediates [9–20]. Although the effects of alkali metal cations have been extensively studied, considerably fewer investigations have focused on multivalent cations, such as alkaline earth metal cations [13, 15, 17, 20, 21], despite both experimental and theoretical indications that Ba^{2+} can outperform smaller divalent cations such as Ca^{2+} [13, 17, 20, 21]. However, the use of alkaline earth metal cations at high concentration in CO_2RR electrolytes—particularly in gas-diffusion electrode systems—remains challenging, as the formation of insoluble carbonate or hydroxide species can hinder CO_2 transport to the catalyst surface [15]. These insights suggest that combining Bi-based catalysts with cations possessing large ionic radii represents a promising approach for selective CO_2RR. Recently, Chang and coworkers investigated cation effects using Bi nanosheets and demonstrated that larger cations, such as Cs^+ and Ba^{2+}, enhance HCOOH productivity and selectivity in acidic electrolytes (pH 2) [20]. Nevertheless, a fundamental understanding of cation effects on Bi-based CO_2RR catalysts remains limited, and strategies to systematically exploit these effects are still at an early stage.

Polyoxometalates (POMs), anionic molecular metal-oxo clusters composed of multiple {MO_x} units (M = W, Mo, V, etc.), are characterized by their structural diversity, compositional tunability, and flexibility in countercation selection, as well as unique physicochemical properties such as acid-base property and multielectron redox property [22–35]. In particular, metal-incorporated POMs enable atomic-level control over active metal species and have emerged as promising (pre)catalysts for CO_2RR as well as components of CO_2RR catalysts [36–39]. Our group has recently demonstrated that the catalytic performance of POM-derived CO_2RR catalysts is highly sensitive to the identity of countercations, with Ba^{2+} significantly enhancing activity and selectivity for carbon monoxide (CO) production [40, 41]. Despite these advances, POM-based CO_2RR catalysts that efficiently produce HCOOH/$HCOO^-$ remain scarcely explored (Tables 1 and S1) [42–45].

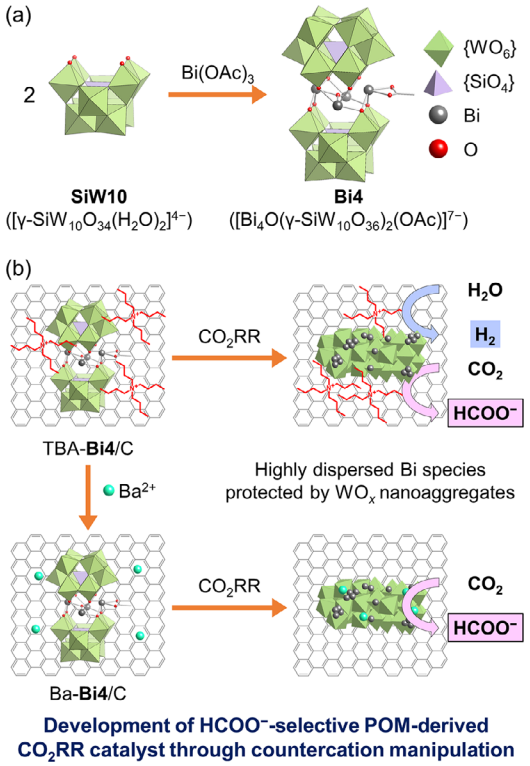


FIGURE 1 | Preparation of POM-derived Bi catalysts and their application in CO_2RR. (a) Synthetic method and the structure of **Bi4** ($[Bi_4O(\gamma\text{-}SiW_{10}O_{36})_2(OAc)]^{7-}$). (b) Schematic illustration of the catalyst preparation and CO_2RR using TBA-**Bi4**/C and Ba-**Bi4**/C.

In this work, we demonstrate that the rational combination of a Bi-incorporated POM and a Ba^{2+} countercation provides an effective strategy for constructing $HCOO^-$-selective CO_2RR catalysts (Figure 1). A Bi-incorporated POM, **Bi4** ($[Bi_4O(\gamma\text{-}SiW_{10}O_{36})_2(OAc)]^{7-}$, Figure 1a) [46], was synthesized by incorporating Bi^{3+} ions into a divacant lacunary POM, **SiW10** ($[\gamma\text{-}SiW_{10}O_{34}(H_2O)_2]^{4-}$) and subsequently immobilized on a carbon support (Figure 1b). The effect of countercation identity was investigated by comparing tetra-*n*-butylammonium (TBA^+), Cs^+, Mg^{2+}, and Ba^{2+} salts. CO_2RR experiments using a gas-fed electrolyzer revealed that the Ba^{2+}-containing catalyst exhibited markedly enhanced $HCOO^-$ production compared with its TBA^+ analogue (Figure 1b). Through a combination of electrochemical analyses, x-ray absorption fine structure analyses, and electron microscopy, we show that the Bi-incorporated POM serves as a molecular precursor that undergoes in situ transformation under CO_2RR conditions to generate highly dispersed Bi species stabilized by WO_x nanoaggregates, while the Ba^{2+} countercation plays a crucial role in directing the reaction selectivity. This study establishes countercation manipulation as a powerful approach for achieving efficient and selective electrochemical $HCOO^-$ production.

2 | Results and Discussion

2.1 | Preparation and Characterization of the Catalysts

Carbon-supported Bi-incorporated POM catalysts were prepared by adapting a previously reported impregnation method for

15213765, 2026, 40, Downloaded from https://chemistry-europe.onlinelibrary.wiley.com/doi/10.1002/chem.71437 by Koji Harano - National Institute For , Wiley Online Library on [28/10/2026]. See the Terms and Conditions (https://onlinelibrary.wiley.com/terms-and-conditions) on Wiley Online Library for rules of use; OA articles are governed by the applicable Creative Commons License

TABLE 1 | Summary of POM-based CO_2RR catalysts exhibiting large $FE_{HCOOH/HCOO-}$ (> 50%).

Catalyst	Electrolyte	Potential	$FE_{HCOOH/HCOO-}$ (%)	$j_{HCOOH/HCOO-}$ (mA cm^{-2})	Reference
Ba-**Bi4**/C	2 M $KHCO_3$	−0.79 V_{RHE}	84.3	33.5	This work
		−0.87 V_{RHE}	68.3	63.9	
Bi-PMo nanosheets	0.5 M $NaHCO_3$	−0.86 V_{RHE}	93 ± 2	ca. 31	[42]
		−1.16 V_{RHE}	ca. 67	ca. 39	
Indium sheet	0.1 M Na_2SO_4 containing 2 mM SiW_9V_3	−1.2 $V_{Ag/AgCl}$ (−0.76 V_{RHE})	<5	<0.2	[43]
		−1.6 $V_{Ag/AgCl}$	56.82	ca. 1.9	
		−1.7 $V_{Ag/AgCl}$	ca. 42	ca. 2.6	
Cu_9S_5 single-unit-cell nanowires[a]	0.1 M $KHCO_3$	−0.8 V_{RHE}	82.0	*ca.* 2.5	[44]
		−0.9 V_{RHE}	57.1	3.20	
$TBA_3H[(Ru(dmbpy)(ppt)Cl)_2P_2W_{17}O_{57}]$[b]	0.1 M $TBAPF_6$-acetonitrile containing acetic acid	−1.56 V_{NHE}	67	—	[45]

[a]Nanowires composed of Cu_9S_5 unit cell and **PW12**.
[b]dmbpy = 4,4'-dimethyl-2,2'-dipyridyl, ppt = 4'-(4-phosphonophenyl)-2,2':6',2''-terpyridine.

POM-derived electrocatalysts [41]. TBA-**Bi4** (Figure 1a) [46] was first immobilized on a carbon support (Vulcan XC 72R), affording TBA-**Bi4**/C (Figure 1b). Subsequently, the countercation of **Bi4** was exchanged from TBA^+ to Ba^{2+}, Mg^{2+}, or Cs^+ by vigorously stirring TBA-**Bi4**/C in an acetone solution containing trifluoromethanesulfonate salts of Ba^{2+}, Mg^{2+}, or Cs^+, yielding Ba-**Bi4**/C, Mg-**Bi4**/C, or Cs-**Bi4**/C, respectively (Figure 1b).

To investigate the structure of **Bi4** after immobilization and cation exchange, Bi and W L_3-edge x-ray absorption fine structure (XAFS) measurements were performed (Figure 2). At the Bi L_3-edge, both TBA-**Bi4**/C and Ba-**Bi4**/C exhibited extended x-ray absorption fine structure (EXAFS) oscillation patterns similar to that of TBA-**Bi4**, indicating preservation of the Bi coordination environment (Figure 2a). Notably, the Fourier-transformed EXAFS spectrum of TBA-**Bi4**/C displayed an increased peak intensity at approximately 1.7 Å (Bi—O bond) relative to that of TBA-**Bi4**, whereas Ba-**Bi4**/C exhibited a slightly lower peak intensity than TBA-**Bi4**/C (Figure 2b). Similarly, at the W L_3-edge, the EXAFS oscillation patterns of TBA-**Bi4**/C and Ba-**Bi4**/C closely resembled those of TBA-**Bi4** (Figure 2c). While TBA-**Bi4** and TBA-**Bi4**/C showed similar Fourier-transformed EXAFS spectra, Ba-**Bi4**/C showed a higher intensity for the peak at approximately 1.3 Å (terminal W═O bond) [47] and a lower intensity for the peak at approximately 1.7 Å (W—O(—W) bond) [47] compared with those of TBA-**Bi4**/C (Figure 2d). These results indicated that immobilization and cation exchange induce only minor perturbations in the local coordination environment of Bi and W, while the overall **Bi4** structure remains largely intact in both TBA-**Bi4**/C and Ba-**Bi4**/C.

Infrared (IR) spectroscopy was further employed to assess the structural integrity of **Bi4** in TBA-**Bi4**/C and Ba-**Bi4**/C. However, due to strong absorption from the carbon support, the characteristic IR absorption bands of **Bi4** could not be observed for

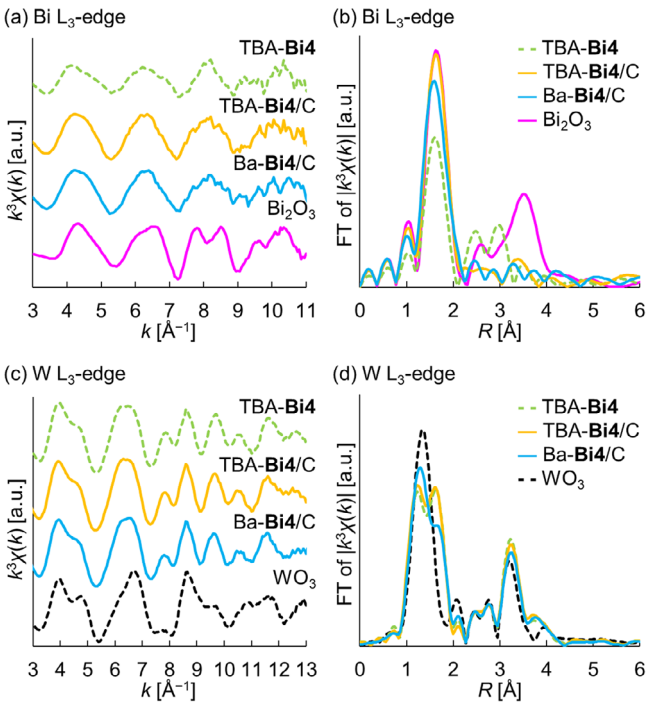


FIGURE 2 | XAFS measurements of TBA-**Bi4**/C and Ba-**Bi4**/C. (a) k^3-weighted Bi L_3-edge EXAFS oscillation. (b) Fourier-transformed Bi L_3-edge EXAFS spectra (k = 3–11 $Å^{-1}$). (c) k^3-weighted W L_3-edge EXAFS oscillation. (d) Fourier-transformed W L_3-edge EXAFS spectra (k = 3–13 $Å^{-1}$).

TBA-**Bi4**/C and Ba-**Bi4**/C. Therefore, IR spectra of unsupported TBA-**Bi4** and Ba-**Bi4** were measured. As shown in Figure S1, Ba-**Bi4** exhibited characteristic absorption bands in the range of 300–1000 cm^{-1} that closely resemble those of TBA-**Bi4**. Importantly, no bands attributable to TBA^+ were observed for Ba-**Bi4** in

15213765, 2026, 40, Downloaded from https://chemistry-europe.onlinelibrary.wiley.com/doi/10.1002/chem.71437 by Koji Harano - National Institute For , Wiley Online Library on [28/10/2026]. See the Terms and Conditions (https://onlinelibrary.wiley.com/terms-and-conditions) on Wiley Online Library for rules of use; OA articles are governed by the applicable Creative Commons License

the range of 1350–1500 cm^{-1}, indicating successful countercation exchange without significant structural change to **Bi4**. Because Ba-**Bi4** was prepared using the same protocol as Ba-**Bi4**/C, these results support effective replacement of TBA^+ with Ba^{2+} in the supported catalyst.

Elemental analysis further confirmed these findings (Table S2). Both TBA-**Bi4**/C and Ba-**Bi4**/C exhibited Bi:W ratios close to 4:20, consistent with the molecular composition of **Bi4** ($[Bi_4O(\gamma\text{-}SiW_{10}O_{36})_2(OAc)]^{7-}$). Moreover, Ba-**Bi4**/C showed a Ba:W ratio of 3.5:20. Considering the heptaanionic charge of **Bi4** and the divalent charge of Ba^{2+}, this ratio supports nearly complete exchange of TBA^+ with Ba^{2+}.

2.2 | CO_2RR Study

The CO_2RR performance of the catalysts was evaluated using a gas-fed electrolyzer equipped with a gas-diffusion electrode (Figure S2). In addition to the **Bi4**-derived catalysts, a Ba^{2+} salt of **SiW10** ($[\gamma\text{-}SiW_{10}O_{34}(H_2O)_2]^{4-}$, a precursor of **Bi4**) supported on carbon (Ba-**SiW10**/C) was prepared as a control sample (see Figure S3 and Table S2 for characterization). The catalyst-loaded electrodes were fabricated by drop-casting catalyst inks onto carbon fiber-based gas-diffusion layer (Sigracet 39 BB, see Supporting Information for detailed methods).

CO_2 electrolysis was conducted at approximately −0.8 V_{RHE} (*iR*-corrected) for 1 h under 80 mL min^{-1} CO_2 flow with 2 M $KHCO_3$ aqueous solution. Gaseous products (CO and H_2) and the water-soluble product ($HCOO^-$) in the catholyte were quantified by gas chromatography and ^1H NMR, respectively. As summarized in Figures 3a and S4a, and Table S3, Ba-**Bi4**/C exhibited the highest partial current density (j_{HCOO-} = 33.5 mA cm^{-2}) and Faradaic efficiency (FE_{HCOO-} = 84.3%) for $HCOO^-$ production among all catalysts tested. No CO or $HCOO^-$ was detected when the bare carbon support was used or when electrolysis was performed under an Ar atmosphere using Ba-**Bi4**/C (Table S4), confirming that these products originate from CO_2RR. Notably, Ba-**Bi4**/C exhibited a j_{HCOO-} value comparable to or higher than those of previously reported POM-based CO_2RR catalysts at similar applied potentials (Table 1). In contrast, Mg-**Bi4**/C, Cs-**Bi4**/C, and TBA-**Bi4**/C exhibited lower CO_2RR performance, with TBA-**Bi4**/C predominantly producing H_2 and showing significantly lower $HCOO^-$ productivity and selectivity (j_{HCOO-} = 9.6 mA cm^{-2}, FE_{HCOO-} = 26.6%), highlighting the importance of selecting appropriate countercations to achieve superior CO_2RR performance. Bismuth(III) acetate ($Bi(OAc)_3$), a precursor of **Bi4**, exhibited an even lower j_{HCOO-} value of 6.1 mA cm^{-2}, although its FE_{HCOO-} was moderate (70.4%) (Figures 3b and S4b and Table S3). In addition, a physical mixture of $Bi(OAc)_3$ and Ba-**SiW10**/C (Ba-**SiW10**/C+$Bi(OAc)_3$) showed low CO_2RR performance. We also evaluated the CO_2RR performance of monolayer bismuth tungstate (Bi_2WO_6), known for efficiently producing $HCOO^-$ [48], and bulk Bi_2WO_6 [49], but both samples exhibited substantially lower productivity and selectivity for $HCOO^-$ production (Figures 3b and S4b and Table S3). These results underscore the critical role of Bi incorporation into the POM framework in achieving high $HCOO^-$-selective CO_2RR performance.

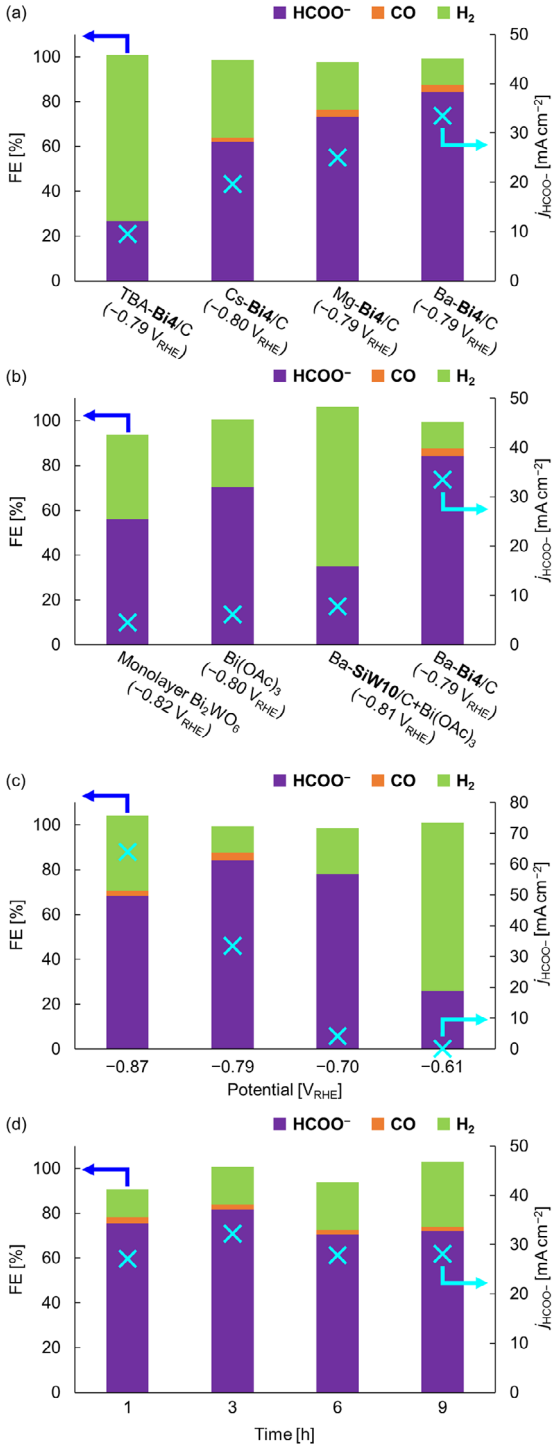


FIGURE 3 | CO_2RR performance of POM-derived catalyst-loaded electrodes with 2 M $KHCO_3$ flow: FE (left axis) and j_{HCOO-} (right axis). (a) **Bi4**/C possessing various countercations at a constant potential around −0.8 V_{RHE} for 1 h. (b) Ba-**Bi4**/C and other benchmark catalysts at a constant potential around −0.8 V_{RHE} for 1 h. (c) Ba-**Bi4**/C at different potentials for 1 h. (d) Ba-**Bi4**/C at −0.82 V_{RHE} for 9 h. All potentials were *iR*-corrected.

Potential-dependent measurements revealed a volcano-type relationship between $HCOO^-$ selectivity and the applied potential for Ba-**Bi4**/C (Figures 3c and S4c and Table S5), with a maximum FE_{HCOO-} of 84.3% observed at −0.79 V_{RHE}. At more negative potentials, the j_{HCOO-} increased further, reaching 63.9 mA cm^{-2}

15213765, 2026, 40, Downloaded from https://chemistry-europe.onlinelibrary.wiley.com/doi/10.1002/chem.71437 by Koji Harano - National Institute For , Wiley Online Library on [28/10/2026]. See the Terms and Conditions (https://onlinelibrary.wiley.com/terms-and-conditions) on Wiley Online Library for rules of use; OA articles are governed by the applicable Creative Commons License

at −0.87 V_{RHE}, representing the highest value reported to date for POM-based CO_2RR catalysts (Table 1). Tafel analysis revealed that the Tafel slope values in the low overpotential region were 55, 54, 63, and 66 mV dec^{-1} for Ba-**Bi4**/C, TBA-**Bi4**/C, Ba-**SiW10**/C+$Bi(OAc)_3$, and $Bi(OAc)_3$, respectively (Figure S5). Notably, these values are close to the theoretical value of 59 mV dec^{-1}, indicating that the protonation of $*CO_2^-$ to form *OCHO is the rate-limiting step across these samples [42, 50–52]. This kinetic similarity suggested that the enhanced $HCOO^-$ productivity of Ba-**Bi4**/C cannot be attributed to a change in the rate-limiting step but to other factors (as discussed in detail in the following sections). Subsequently, long-term CO_2RR electrolysis was conducted at −0.82 V_{RHE} for 9 h using Ba-**Bi4**/C (Figures 3d and S4d,e and Table S6). Although the selectivity to H_2 gradually increased during the prolonged electrolysis, the FE_{HCOO-} remained above 70% even after 9 h, and the j_{HCOO-} remained nearly constant throughout the experiment. In addition, although the slight fluctuations were observed during the initial 4 h, the total current density stabilized at approximately 40 mA cm^{-2} thereafter, demonstrating the robust electrochemical stability of the catalyst.

2.3 | Characterization of a Ba-Bi4/C-Loaded Electrode After CO_2RR

Based on the above results, we next discuss the structural evolution of Ba-**Bi4**/C under CO_2RR conditions.

We first performed XAFS measurements on Ba-**Bi4**/C electrodes before and after immersion in the catholyte (2 M $KHCO_3$) for 1 h to examine the effect of catholyte contact on the electronic state and the structure of **Bi4**. As displayed in Figure 4, both electrodes exhibited x-ray absorption near edge structure (XANES) spectra (Figure 4a) and EXAFS oscillation patterns that closely resemble those of pristine Ba-**Bi4**/C (Figure 4b,d), although slight variations in the peak intensities associated with the Bi—O bond (peak around 1.7 Å, Figure 4c), the terminal W═O bond (peak around 1.3 Å, Figure 4e) [47], and the W—O(—W) bond (peak around 1.7 Å, Figure 4e) [47] were observed. These results suggest that, although minor perturbations occurred during electrode fabrication and catholyte contact, the overall electronic state and the molecular structure of **Bi4** were largely retained.

To identify the catalytically active Bi species generated under CO_2RR conditions, cyclic voltammetry (CV) of the Ba-**Bi4**/C electrode after CO_2RR at −0.8 V_{RHE} for 1 h was conducted (Figure S6). A single cathodic peak appeared in the range of 0.1–0.2 V_{RHE}, which can be assigned to the reduction of Bi^{3+} to Bi^0 [53]. Given that CO_2RR was conducted at much more negative potentials (approximately −0.8 V_{RHE}), Bi^0 species were likely generated during electrolysis and served as the truly catalytically active sites.

Further insight into the post-reaction catalyst structure was obtained by XAFS measurements of the Ba-**Bi4**/C electrode after CO_2RR (Figure 4). The Bi L_3-edge XANES spectrum of the post-reaction electrode closely overlapped with those of pristine Ba-**Bi4**/C and the electrode before the reaction, indicating that Bi was predominantly present as Bi^{3+} after the reaction (Figure 4a). This observation does not contradict the CV results, as the ex situ XAFS measurements were performed after exposure of the

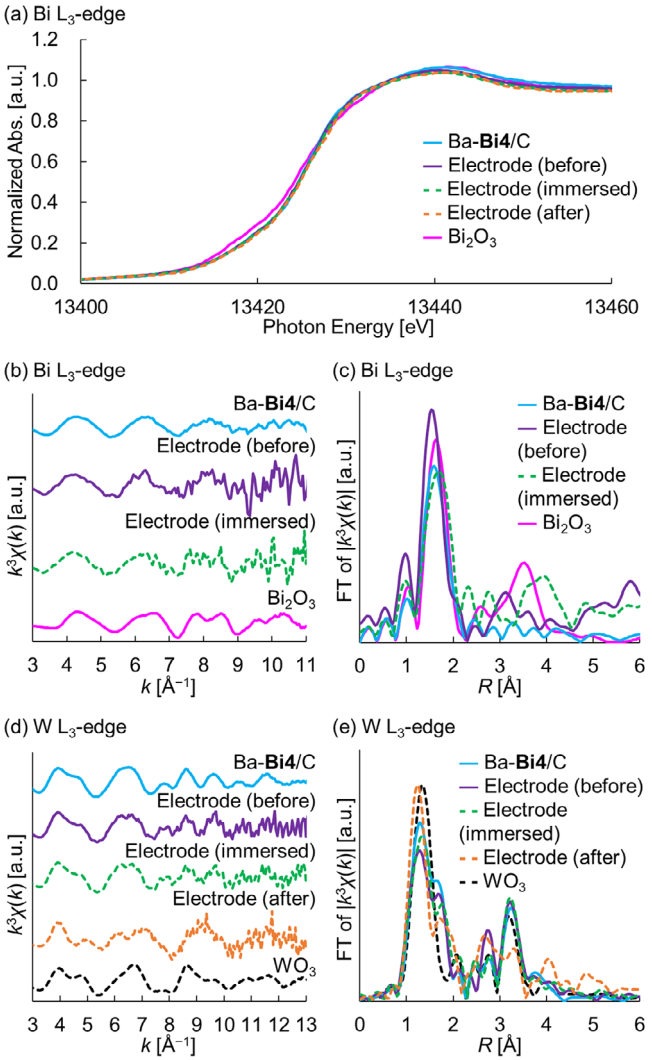


FIGURE 4 | XAFS measurements of Ba-**Bi4**/C-loaded electrodes. (a) Bi L_3-edge XANES spectra. (b) k^3-weighted Bi L_3-edge EXAFS oscillation. (c) Fourier-transformed Bi L_3-edge EXAFS spectra (k = 3–11 $Å^{-1}$). (d) k^3-weighted W L_3-edge EXAFS oscillation. (e) Fourier-transformed W L_3-edge EXAFS spectra (k = 3–13 $Å^{-1}$).

electrode to air, which can readily oxidize metallic Bi. At the W L_3-edge, the EXAFS oscillation pattern of the electrode after CO_2RR more closely resembled that of WO_3 than that of the electrode before the reaction; however, clear differences were observed in the k range of 7–9 $Å^{-1}$ and in the Fourier-transformed spectra around 3–4 Å (Figure 4d,e). These features suggest the formation of WO_x species distinct from bulk WO_3 during CO_2RR.

To further elucidate the nanoscale structure of the catalyst after CO_2RR, electron microscopy analysis was performed. We initially carried out atomic-resolution transmission electron microscopy (TEM) observation of the Ba-**Bi4**/C electrode after a 1 h CO_2RR (Figure S7). However, the detailed analysis of catalyst morphology was difficult due to the low contrast between the carbon support and the catalyst. High-angle annular dark-field scanning transmission electron microscopy (HAADF-STEM) image (Figure 5a) and the corresponding STEM energy-dispersive X-ray spectroscopy (EDS) mappings (Figure 5b–e) suggest the formation of WO_x nanoaggregates within which Bi species are

15213765, 2026, 40, Downloaded from https://chemistry-europe.onlinelibrary.wiley.com/doi/10.1002/chem.71437 by Koji Harano - National Institute For , Wiley Online Library on [28/10/2026]. See the Terms and Conditions (https://onlinelibrary.wiley.com/terms-and-conditions) on Wiley Online Library for rules of use; OA articles are governed by the applicable Creative Commons License

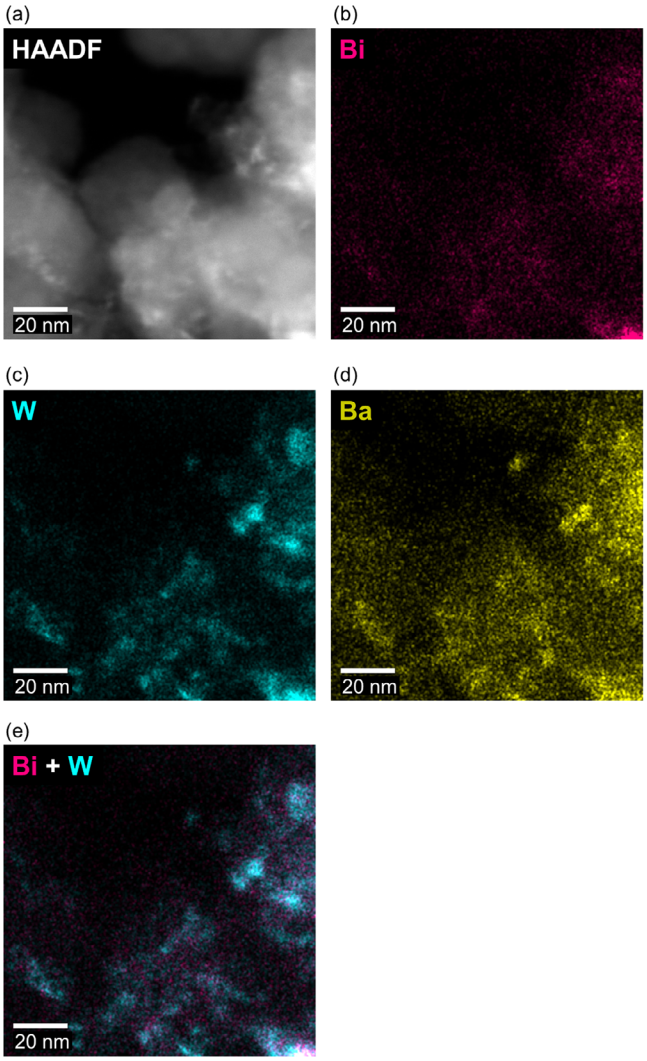


FIGURE 5 | STEM images of Ba-**Bi4**/C-loaded electrode after a 1 h CO_2RR. (a) HAADF-STEM image and (b–e) STEM-EDS mappings (Bi, magenta; W, cyan; Ba, yellow).

highly dispersed. Although some Bi species formed nanoparticles within WO_x nanoaggregates (Figure S8), low-magnification STEM images also verified that most of the Bi species were highly dispersed (Figure S9). Liu and coworkers reported that, under CO_2RR conditions, monolayer bismuth tungstate (Bi_2WO_6) reconstructs to form metallic Bi stabilized by tungsten oxide species, as revealed by in situ characterization techniques [48]. In light of this report, it is reasonable to conclude that, in the present system, Bi species are likewise stabilized by WO_x nanoaggregates.

Taken together, the CV, XAFS, and STEM results demonstrate that Ba-**Bi4**/C is transformed into highly dispersed Bi species protected by WO_x nanoaggregates under CO_2RR conditions.

2.4 | Effect of Countercations on CO_2RR Performance

As shown in the former section, TBA-**Bi4**/C exhibited substantially lower CO_2RR performance than Ba-**Bi4**/C. In this section, we discuss the role of countercation in determining the CO_2RR performance.

Post-reaction characterization of the TBA-**Bi4**/C electrode after CO_2RR at −0.8 V_{RHE} was first conducted. CV measurement revealed a cathodic peak in the range of 0.1–0.2 V_{RHE} corresponding to the reduction of Bi^{3+} to Bi^0, indicating that Bi^0 is also generated as the active species under CO_2RR conditions (Figure S6). XAFS analysis further clarified that the Bi L_3-edge XANES spectra and W L_3-edge EXAFS oscillation patterns of TBA-**Bi4**/C and Ba-**Bi4**/C electrodes after the reaction were largely comparable, with only minor differences observed in the Fourier-transformed W L_3-edge EXAFS spectra (Figure S10). Consistent with these results, STEM analysis revealed the formation of highly dispersed Bi species protected by WO_x nanoaggregates on the TBA-**Bi4**/C electrode after the reaction (Figure S11). These observations suggest that both catalysts underwent similar structural transformations during CO_2RR. Elemental analysis was performed to quantify the Bi content remaining on the electrodes after reaction. As summarized in Table S7, although initial Bi loadings were nearly identical for both samples, the Ba-**Bi4**/C electrode after the reaction exhibited a slightly lower Bi loading than the TBA-**Bi4**/C electrode after the reaction. This result suggests that differences in Bi loading are unlikely to be the primary origin of the large performance difference.

It has been reported that electron-rich Bi-based CO_2RR catalysts tend to exhibit higher CO_2RR performance, as electron-rich Bi sites facilitate either the reduction of *OCHO intermediates or the formation of $*CO_2^-$ intermediates [54, 55]. To assess the electronic state of Bi, CV measurements were performed on TBA-**Bi4**/C and Ba-**Bi4**/C electrodes after the reaction (Figure S6). Notably, the reduction peak of Bi^{3+} for the TBA-**Bi4**/C electrode appeared at a potential approximately 10 mV more negative than that for the Ba-**Bi4**/C electrode. Chen and coworkers reported a correlation among the reduction potential of Bi^{3+}, the electronic state of Bi, and the CO_2RR performance, demonstrating that more electron-rich Bi species exhibit more negative reduction potentials and higher CO_2RR activity [54]. Accordingly, TBA-**Bi4**/C appears to generate slightly more electron-rich Bi species, consistent with our previous report [40]. This difference may originate from countercation-dependent electron-donating properties of the WO_x nanoaggregates.

Importantly, despite possessing slightly more electron-rich species, TBA-**Bi4**/C exhibited inferior CO_2RR performance. This finding indicates that electronic effects cannot account for the enhanced CO_2RR performance of Ba-**Bi4**/C. We therefore attribute the superior performance of Ba-**Bi4**/C primarily to cation effects. Although the origin of cation effects in CO_2RR remains under debate, three main contributions have been proposed: (a) modulation of the electric field near the electrode surface; (b) buffering of the local pH near the electrode surface; and (c) stabilization of reaction intermediates [56–59]. While it is difficult to unambiguously identify the dominant factor in the present system, it is reasonable to conclude that Ba^{2+}-induced cation effects play a critical role in enhancing the CO_2RR performance of Ba-**Bi4**/C.

2.5 | Effect of Catalyst Structure on CO_2RR Performance

As described in the CO_2RR Study Section, $Bi(OAc)_3$ exhibited significantly lower CO_2RR performance than Ba-**Bi4**/C. In this

15213765, 2026, 40, Downloaded from https://chemistry-europe.onlinelibrary.wiley.com/doi/10.1002/chem.71437 by Koji Harano - National Institute For , Wiley Online Library on [28/10/2026]. See the Terms and Conditions (https://onlinelibrary.wiley.com/terms-and-conditions) on Wiley Online Library for rules of use; OA articles are governed by the applicable Creative Commons License

section, we discuss the influence of the catalyst structure on CO_2RR performance.

After CO_2RR at −0.8 V_{RHE} for 1 h, CV analysis of the $Bi(OAc)_3$-derived electrode revealed a reduction peak corresponding to the conversion of Bi^{3+} to Bi^0 in the range of 0.0–0.3 V_{RHE}, indicating that Bi^0 species also serve as the active species in this system (Figure S6). Ex situ XAFS measurement suggested that in situ-generated Bi^0 species were fully oxidized to Bi^{3+} after the reaction (Figure S12). TEM analysis further revealed the formation of Bi nanoparticles with an average diameter of 2.9 ± 1.2 nm after the reaction (Figure S13). These outcomes all suggest that $Bi(OAc)_3$ is transformed into small Bi nanoparticles during the reaction. Elemental analysis (Table S7) showed that the Bi content remaining on the $Bi(OAc)_3$ electrode after CO_2RR was approximately twice that on the Ba-**Bi4**/C electrode after the reaction, suggesting that the inferior CO_2RR performance observed for $Bi(OAc)_3$ may not stem from lower Bi loading.

CV measurements comparing the electronic states of Bi species formed on $Bi(OAc)_3$ and Ba-**Bi4**/C electrodes after reaction showed that the reduction peak for Ba-**Bi4**/C shifted by approximately 10 mV to a more negative potential, suggesting the formation of slightly more electron-rich Bi species (Figure S6). However, given the small magnitude of this shift, electronic effects are unlikely to be the dominant factor governing the observed performance difference. Instead, we attribute the superior performance of Ba-**Bi4**/C primarily to its ability to generate and stabilize highly dispersed Bi species. The electrochemical impedance spectroscopy at −0.8 V_{RHE} revealed that the catalyst derived from Ba-**Bi4**/C exhibited significantly lower charge transfer resistance than that derived from $Bi(OAc)_3$ (Figure S14). The close proximity between Bi and $\{WO_6\}$ units in Ba-**Bi4**/C facilitates the formation of isolated or highly dispersed Bi species stabilized by WO_x nanoaggregates, whereas $Bi(OAc)_3$, lacking such protection by WO_x species, readily aggregates into Bi nanoparticles. As a consequence, Ba-**Bi4**/C showed faster electron transfer kinetics and higher CO_2RR performance.

3 | Conclusion

In this study, we demonstrated that countercation manipulation provides a facile and powerful strategy for tuning the performance of POM-based electrocatalysts for CO_2RR. A bismuth (Bi)-incorporated POM, $[Bi_4O(\gamma\text{-}SiW_{10}O_{36})_2(OAc)]^{7-}$ (**Bi4**), was immobilized on a carbon support via an impregnation method to afford TBA-**Bi4**/C, followed by countercation exchange with Ba^{2+} to yield Ba-**Bi4**/C. When evaluated as gas-diffusion electrodes in a gas-fed CO_2 electrolyzer using 2 M $KHCO_3$ aqueous electrolyte, Ba-**Bi4**/C exhibited markedly enhanced formate ($HCOO^-$) production, achieving a high partial current density (j_{HCOO-} = 33.5 mA cm^{-2}) and Faradaic efficiency (FE_{HCOO-} = 84.3%) at −0.79 V_{RHE}. In contrast, TBA-**Bi4**/C showed significantly lower $HCOO^-$ selectivity (FE_{HCOO-} = 26.6% at −0.79 V_{RHE}), while $Bi(OAc)_3$, a precursor of **Bi4**, exhibited lower $HCOO^-$ productivity (j_{HCOO-} = 6.1 mA cm^{-2}). Post-reaction analyses revealed that both Ba-**Bi4**/C and TBA-**Bi4**/C underwent in situ structural reconstruction during CO_2RR to form highly dispersed Bi species stabilized by WO_x nanoaggregates, whereas $Bi(OAc)_3$ was transformed into aggregated Bi nanoparticles. Systematic control experiments and characterizations highlighted the critical roles of both countercation identity and molecular structure of the precatalyst in achieving high CO_2RR performance, underscoring countercation manipulation as a key design parameter.

Given that $HCOO^-$-selective POM-based CO_2RR catalysts remain scarce and the role of cations in Bi-based CO_2RR catalysis is still not fully understood, this work provides new insights into cation effects and establishes a generalizable strategy for designing efficient POM-based CO_2RR catalysts. We anticipate that the concept of countercation engineering demonstrated here will inspire further development of molecularly defined electrocatalysts for selective and efficient CO_2 conversion.

Acknowledgments

This work was financially supported by the JSPS KAKENHI (Grant JP24K01448, JP24H00463, JP24H02210, JP24H02217, JP22H04971, JP23H04874) and the JST FOREST (JPMJFR213M). A part of this work was supported by Advanced Research Infrastructure for Materials and Nanotechnology in Japan (ARIM) (JPMXP1225NM0211, JPMXP12 25UT0269) of the Ministry of Education, Culture, Sports, Science and Technology (MEXT). A part of this study was supported by Advanced Engineering and Services Division in National Institute for Materials Science (NIMS). The authors thank Dr. Fumihiko Uesugi (NIMS), Mr. Kouichi Okudaira (NIMS), Mr. Hiroyuki Oshikawa (The University of Tokyo), and Ms. Mari Morita (The University of Tokyo) for the assistance with TEM, HAADF-STEM, and EDS analyses. XAFS measurements using a CITIUS detector were performed at BL36XU in SPring-8 under an approved SACLA/SPring-8 Basic Development Program proposal (No. 202407 and No. 202505).

Funding

Japan Science and Technology Agency. Japan Society for the Promotion of Science

Conflicts of Interest

The authors declare no conflicts of interest.

Data Availability Statement

The data that support the findings of this study are available in the Supporting Information of this article.

References

1. V. Masson-Delmotte, P. Zhai, A. Pirani, et al., IPCC "*Climate Change 2021: The Physical Science Basis*," Contribution of Working Group I to the Sixth Assessment Report of the Intergovernmental Panel on Climate Change, (Cambridge University Press): 2021.

2. Z. Sun, T. Ma, H. Tao, Q. Fan, and B. Han, "Fundamentals and Challenges of Electrochemical CO_2 Reduction Using Two-Dimensional Materials," *Chem* 3 (2017): 560, https://doi.org/10.1016/j.chempr.2017.09.009.

3. S. Nitopi, E. Bertheussen, S. B. Scott, et al., "Progress and Perspectives of Electrochemical CO_2 Reduction on Copper in Aqueous Electrolyte," *Chemical Reviews* 119 (2019): 7610, https://doi.org/10.1021/acs.chemrev.8b00705.

4. J. Hietala, A. Vuori, P. Johnsson, I. Pollari, W. Reutemann, and H. Kieczka, *Formic Acid, Ullmann's Encyclopedia of Industrial Chemistry* (Wiley-VCH Verlag, 2016), https://doi.org/10.1002/14356007.a12_013.pub3.

15213765, 2026, 40, Downloaded from https://chemistry-europe.onlinelibrary.wiley.com/doi/10.1002/chem.71437 by Koji Harano - National Institute For , Wiley Online Library on [28/10/2026]. See the Terms and Conditions (https://onlinelibrary.wiley.com/terms-and-conditions) on Wiley Online Library for rules of use; OA articles are governed by the applicable Creative Commons License

5. H. Zhong, M. Iguchi, M. Chatterjee, Y. Himeda, Q. Xu, and H. Kawanami, "Formic Acid-Based Liquid Organic Hydrogen Carrier System With Heterogeneous Catalysts," *Advanced Sustainable Systems* 2 (2018): 1700161, https://doi.org/10.1002/adsu.201700161.

6. M. Jouny, W. Luc, and F. Jiao, "General Techno-Economic Analysis of CO_2 Electrolysis Systems," *Industrial & Engineering Chemistry Research* 57 (2018): 2165, https://doi.org/10.1021/acs.iecr.7b03514.

7. D. Xia, H. Yu, H. Xie, et al., "Recent Progress of Bi-Based Electrocatalysts for Electrocatalytic CO_2 Reduction," *Nanoscale* 14 (2022): 7957, https://doi.org/10.1039/D2NR01900K.

8. X.-D. Liang, N. Tian, S.-N. Hu, Z.-Y. Zhou, and S.-G. Sun, "Recent Advances of Bismuth-Based Electrocatalysts for CO_2 Reduction: Strategies, Mechanism and Applications," *Materials Reports Energy* 3 (2023): 100191, https://doi.org/10.1016/j.matre.2023.100191.

9. A. Murata and Y. Hori, "Product Selectivity Affected by Cationic Species in Electrochemical Reduction of CO_2 and CO at a Cu Electrode," *Bulletin of the Chemical Society of Japan* 64 (1991): 123, https://doi.org/10.1246/bcsj.64.123.

10. M. R. Thorson, K. I. Siil, and P. J. A. Kenis, "Effect of Cations on the Electrochemical Conversion of CO_2 to CO," *Journal of the Electrochemical Society* 160 (2012): F69, https://doi.org/10.1149/2.052301jes.

11. M. R. Singh, Y. Kwon, Y. Lum, J. W. Ager, and A. T. Bell, "Hydrolysis of Electrolyte Cations Enhances the Electrochemical Reduction of CO_2 Over Ag and Cu," *Journal of the American Chemical Society* 138 (2016): 13006, https://doi.org/10.1021/jacs.6b07612.

12. J. Resasco, L. D. Chen, E. Clark, et al., "Promoter Effects of Alkali Metal Cations on the Electrochemical Reduction of Carbon Dioxide," *Journal of the American Chemical Society* 139 (2017): 11277, https://doi.org/10.1021/jacs.7b06765.

13. S. Ringe, E. L. Clark, J. Resasco, et al., "Understanding Cation Effects in Electrochemical CO_2 Reduction," *Energy & Environmental Science* 12 (2019): 3001, https://doi.org/10.1039/C9EE01341E.

14. A. S. Malkani, J. Anibal, and B. Xu, "Cation Effect on Interfacial CO_2 Concentration in the Electrochemical CO_2 Reduction Reaction," *ACS Catalysis* 10 (2020): 14871, https://doi.org/10.1021/acscatal.0c03553.

15. S. S. Bhargava, E. R. Cofell, P. Chumble, D. Azmoodeh, S. Someshwar, and P. J. A. Kenis, "Exploring Multivalent Cations-Based Electrolytes for CO_2 Electroreduction," *Electrochimica Acta* 394 (2021): 139055, https://doi.org/10.1016/j.electacta.2021.139055.

16. M. C. O. Monteiro, F. Dattila, B. Hagedoorn, R. García-Muelas, N. López, and M. T. M. Koper, "Absence of CO_2 Electroreduction on Copper, Gold and Silver Electrodes Without Metal Cations in Solution," *Nature Catalysis* 4 (2021): 654, https://doi.org/10.1038/s41929-021-00655-5.

17. M. C. O. Monteiro, F. Dattila, N. López, and M. T. M. Koper, "The Role of Cation Acidity on the Competition Between Hydrogen Evolution and CO_2 Reduction on Gold Electrodes," *Journal of the American Chemical Society* 144 (2022): 1589, https://doi.org/10.1021/jacs.1c10171.

18. J. Gu, S. Liu, W. Ni, W. Ren, S. Haussener, and X. Hu, "Modulating Electric Field Distribution by Alkali Cations for CO_2 Electroreduction in Strongly Acidic Medium," *Nature Catalysis* 5 (2022): 268, https://doi.org/10.1038/s41929-022-00761-y.

19. T.-W. Jiang, S.-S. Wang, X. Qin, et al., "Uncovering the Cation Effects on the Electroreduction of CO_2 on Pd/C Catalysts – An SEIRAS Study," *Journal of Catalysis* 434 (2024): 115520, https://doi.org/10.1016/j.jcat.2024.115520.

20. Y. Chang, Z. Tan, J. Han, et al., "Effect of Alkali and Alkaline Earth Metal Cations on the HCOOH Selectivity of the CO_2 Electrochemical Reduction Reaction on Bi Electrodes in Acidic media," *Journal of Alloys and Compounds* 1035 (2025): 181524, https://doi.org/10.1016/j.jallcom.2025.181524.

21. A. Schizodimou and G. Kyriacou, "Acceleration of the Reduction of Carbon Dioxide in the Presence of Multivalent Cations," *Electrochimica Acta* 78 (2012): 171, https://doi.org/10.1016/j.electacta.2012.05.118.

22. M. T. Pope, *Heteropoly and Isopoly Oxometalates* (Springer, 1983), https://link.springer.com/book/9783662120064.

23. C. L. Hill and C. M. Prosser-McCartha, "Homogeneous Catalysis by Transition Metal Oxygen Anion Clusters," *Coordination Chemistry Reviews* 143 (1995): 407, https://doi.org/10.1016/0010-8545(95)01141-B.

24. I. V. Kozhevnikov, "Catalysis by Heteropoly Acids and Multicomponent Polyoxometalates in Liquid-Phase Reactions," *Chemical Reviews* 98 (1998): 171, https://doi.org/10.1021/cr960400y.

25. N. Mizuno and M. Misono, "Heterogeneous Catalysis," *Chemical Reviews* 98 (1998): 199, https://doi.org/10.1021/cr960401q.

26. A. Dolbecq, E. Dumas, C. R. Mayer, and P. Mialane, "Hybrid Organic–Inorganic Polyoxometalate Compounds: From Structural Diversity to Applications," *Chemical Reviews* 110 (2010): 6009, https://doi.org/10.1021/cr1000578.

27. S.-S. Wang and G.-Y. Yang, "Recent Advances in Polyoxometalate-Catalyzed Reactions," *Chemical Reviews* 115 (2015): 4893, https://doi.org/10.1021/cr500390v.

28. L. Vilà-Nadal and L. Cronin, "Design and Synthesis of Polyoxometalate-Framework Materials From Cluster Precursors," *Nature Reviews Materials* 2 (2017): 17054, https://doi.org/10.1038/natrevmats.2017.54.

29. N. I. Gumerova and A. Rompel, "Synthesis, Structures and Applications of Electron-Rich Polyoxometalates," *Nature Reviews Chemistry* 2 (2018): 0112, https://doi.org/10.1038/s41570-018-0112.

30. K. Suzuki, N. Mizuno, and K. Yamaguchi, "Polyoxometalate Photocatalysis for Liquid-Phase Selective Organic Functional Group Transformations," *ACS Catalysis* 8 (2018): 10809, https://doi.org/10.1021/acscatal.8b03498.

31. A. Misra, K. Kozma, C. Streb, and M. Nyman, "Beyond Charge Balance: Counter-Cations in Polyoxometalate Chemistry," *Angewandte Chemie International Edition* 59 (2020): 596, https://doi.org/10.1002/anie.201905600.

32. B. Fabre, C. Falaise, and E. Cadot, "Polyoxometalates-Functionalized Electrodes for (Photo)Electrocatalytic Applications: Recent Advances and Prospects," *ACS Catalysis* 12 (2022): 12055, https://doi.org/10.1021/acscatal.2c01847.

33. J.-H. Kruse, M. Langer, I. Romanenko, et al., "Polyoxometalate-Soft Matter Composite Materials: Design Strategies, Applications, and Future Directions," *Advanced Functional Materials* 32 (2022): 2208428, https://doi.org/10.1002/adfm.202208428.

34. J. M. Cameron, G. Guillemot, T. Galambos, et al., "Supramolecular Assemblies of Organo-Functionalised Hybrid Polyoxometalates: From Functional Building Blocks to Hierarchical Nanomaterials," *Chemical Society Reviews* 51 (2022): 293, https://doi.org/10.1039/D1CS00832C.

35. C. Falaise, "Super-Reduced Polyoxometalates in Aqueous Solution: Historical Perspectives and Current Challenges," *European Journal of Inorganic Chemistry* 28 (2025): e202400827, https://doi.org/10.1002/ejic.202400827.

36. D. Azaiza-Dabbah, C. Vogt, F. Wang, et al., "Molecular Transition Metal Oxide Electrocatalysts for the Reversible Carbon Dioxide–Carbon Monoxide Transformation," *Angewandte Chemie International Edition* 61 (2022): e202112915, https://doi.org/10.1002/anie.202112915.

37. D. Azaiza-Dabbah, F. Wang, E. Haddad, et al., "Heterometallic Transition Metal Oxides Containing Lewis Acids as Molecular Catalysts for the Reduction of Carbon Dioxide to Carbon Monoxide With Bimodal Activity," *Journal of the American Chemical Society* 146 (2024): 27871, https://doi.org/10.1021/jacs.4c10412.

38. M.-L. Sun, Y.-R. Wang, W.-W. He, et al., "Efficient Electron Transfer From Electron-Sponge Polyoxometalate to Single-Metal Site Metal–Organic Frameworks for Highly Selective Electroreduction of Carbon Dioxide," *Small* 17 (2021): 2100762, https://doi.org/10.1002/smll.202100762.

15213765, 2026, 40, Downloaded from https://chemistry-europe.onlinelibrary.wiley.com/doi/10.1002/chem.71437 by Koji Harano - National Institute For , Wiley Online Library on [28/10/2026]. See the Terms and Conditions (https://onlinelibrary.wiley.com/terms-and-conditions) on Wiley Online Library for rules of use; OA articles are governed by the applicable Creative Commons License

39. C. Li, Y. Zhang, L. Shu, Y.-L. Teng, Y.-R. Wang, and B.-X. Dong, "Boosting Electrochemical Reduction of CO_2 to CO via Fixation Keggin-Type Polyoxoanions $XW_{11}Co$ (X = Si, P, Co) Into ZIF-8 Cavities: Pivotal Role of Central Atoms in Catalytic Performance," *Polyoxometalates* 4 (2025): 9140097, https://doi.org/10.26599/POM.2025.9140097.

40. K. Kawakami, T. Yabe, F. Amano, K. Yamaguchi, and K. Suzuki, "Pd-incorporated Polyoxometalate Catalysts for Electrochemical CO_2 Reduction," *Chemical Science* 15 (2024): 14829, https://doi.org/10.1039/D4SC04304A.

41. K. Kawakami, K. Yonesato, S. Kikkawa, et al., "Polyoxometalate-Based Au–Ag Alloy Nanocatalysts for Efficient Electrochemical CO_2 Reduction Reaction," *ChemCatChem* 18 (2026): e01423, https://doi.org/10.1002/cctc.202501423.

42. S.-X. Guo, Y. Zhang, X. Zhang, C. D. Easton, D. R. MacFarlane, and J. Zhang, "Phosphomolybdic Acid-Assisted Growth of Ultrathin Bismuth Nanosheets for Enhanced Electrocatalytic Reduction of CO_2 to Formate," *ChemSusChem* 12 (2019): 1091, https://doi.org/10.1002/cssc.201802409.

43. B. Zha, C. Li, and J. Li, "Efficient Electrochemical Reduction of CO_2 Into Formate and Acetate in Polyoxometalate Catholyte With Indium Catalyst," *Journal of Catalysis* 382 (2020): 69, https://doi.org/10.1016/j.jcat.2019.12.010.

44. D. Yang, S. Zuo, H. Yang, and X. Wang, "Single-Unit-Cell Catalysis of CO_2 Electroreduction Over Sub-1 Nm Cu_9S_5 Nanowires," *Advanced Energy Materials* 11 (2021): 2100272, https://doi.org/10.1002/aenm.202100272.

45. S. Kuramochi, J. M. Cameron, T. Fukui, et al., "Selective Electrochemical CO_2 Conversion With a Hybrid Polyoxometalate," *Chemical Communications* 59 (2023): 10801, https://doi.org/10.1039/D3CC02138F.

46. T. Hanaya, K. Suzuki, R. Sato, K. Yamaguchi, and N. Mizuno, "Creation of Bismuth–Tungsten Oxide Nanoclusters Using Lacunary Polyoxometalates," *Dalton Transactions* 46 (2017): 7384, https://doi.org/10.1039/C7DT01587A.

47. J. Evans, M. Pillinger, and J. M. Rummey, "Applications of Extended X-Ray Absorption Fine Structure Spectroscopy to the Study of Polyoxometalates," *Journal of the Chemical Society, Dalton Transactions*25 (1996): 2951, https://doi.org/10.1039/DT9960002951.

48. S. Liu, C. Wang, J. Wu, et al., "Efficient CO_2 Electroreduction With a Monolayer Bi_2WO_6 Through a Metallic Intermediate Surface State," *ACS Catalysis* 11 (2021): 12476, https://doi.org/10.1021/acscatal.1c02495.

49. H. Hori, M. Takase, F. Amano, and B. Ohtani, "Mechanism of the Formation of Hierarchical-Structured Bismuth Tungstate Photocatalyst Particles Through Counter-Flow Supply of Bismuth and Tungsten Sources," *Chemistry Letters* 44 (2015): 1723, https://doi.org/10.1246/cl.150893.

50. X. Zhang, X. Sun, S.-X. Guo, A. M. Bond, and J. Zhang, "Formation of Lattice-Dislocated Bismuth Nanowires on Copper Foam for Enhanced Electrocatalytic CO_2 Reduction at Low Overpotential," *Energy & Environmental Science* 12 (2019): 1334, https://doi.org/10.1039/C9EE00018F.

51. T. Fan, W. Ma, M. Xie, et al., "Achieving High Current Density for Electrocatalytic Reduction of CO_2 to Formate on Bismuth-Based Catalysts," *Cell Reports Physical Science* 2 (2021): 100353, https://doi.org/10.1016/j.xcrp.2021.100353.

52. P.-F. Sui, M.-R. Gao, M.-N. Zhu, et al., "Unlocking Nanotubular Bismuth Oxyiodide Toward Carbon-Neutral Electrosynthesis," *EES Catalysis* 1 (2023): 290, https://doi.org/10.1039/D3EY00034F.

53. X. Huang, X. Han, R. Tang, et al., "Anion-Mediated *In Situ* Reconstruction of the Bi_2MoO_6 Precatalyst for Enhanced Electrochemical CO_2 Reduction Over a Wide Potential Window," *ACS Applied Materials & Interfaces* 16 (2024): 742, https://doi.org/10.1021/acsami.3c14930.

54. X. Chen, H. Chen, W. Zhou, et al., "Boron Dopant Induced Electron-Rich Bismuth for Electrochemical CO_2 Reduction With High Solar Energy Conversion Efficiency," *Small* 17 (2021): 2101128, https://doi.org/10.1002/smll.202101128.

55. Z. Li, B. Sun, D. Xiao, et al., "Electron-Rich Bi Nanosheets Promote $CO_2^{\cdot-}$ Formation for High-Performance and pH-Universal Electrocatalytic CO_2 Reduction," *Angewandte Chemie International Edition* 62 (2023): e202217569, https://doi.org/10.1002/anie.202217569.

56. M. Moura de Salles Pupo and R. Kortlever, "Electrolyte Effects on the Electrochemical Reduction of CO_2," *ChemPhysChem* 20 (2019): 2926, https://doi.org/10.1002/cphc.201900680.

57. G. Marcandalli, M. C. O. Monteiro, A. Goyal, and M. T. M. Koper, "Electrolyte Effects on CO_2 Electrochemical Reduction to CO," *Accounts of Chemical Research* 55 (2022): 1900, https://doi.org/10.1021/acs.accounts.2c00080.

58. B. Deng, M. Huang, X. Zhao, S. Mou, and F. Dong, "Interfacial Electrolyte Effects on Electrocatalytic CO_2 Reduction," *ACS Catalysis* 12 (2022): 331, https://doi.org/10.1021/acscatal.1c03501.

59. H. Khani, A. R. Puente Santiago, and T. He, "An Interfacial View of Cation Effects on Electrocatalysis Systems," *Angewandte Chemie International Edition* 62 (2023): e202306103, https://doi.org/10.1002/anie.202306103.

60. K. P. Kuhl, E. R. Cave, D. N. Abram, and T. F. Jaramillo, "New Insights Into the Electrochemical Reduction of Carbon Dioxide on Metallic Copper Surfaces," *Energy & Environmental Science* 5 (2012): 7050, https://doi.org/10.1039/C2EE21234J.

61. K. Kamata, K. Yonehara, Y. Sumida, K. Yamaguchi, S. Hikichi, and N. Mizuno, "Efficient Epoxidation of Olefins With ≥99% Selectivity and Use of Hydrogen Peroxide," *Science* 300 (2003): 964, https://doi.org/10.1126/science.1083176.

62. T. Suzuki, T. Yabe, K. Wachi, K. Yonesato, K. Suzuki, and K. Yamaguchi, "Creation of Highly Dispersed Supported Polyoxometalate Cesium Salts via Cation Exchange From Alkylammonium Salts on Supports," *ChemNanoMat* 9 (2023): e202200428, https://doi.org/10.1002/cnma.202200428.

63. S. Gonglach, S. Paul, M. Haas, et al., "Molecular Cobalt Corrole Complex for the Heterogeneous Electrocatalytic Reduction of Carbon Dioxide," *Nature Communications* 10 (2019): 3864, https://doi.org/10.1038/s41467-019-11868-5.

64. Y. Takahashi, M. Abe, H. Uematsu, et al., "High-Resolution and High-Sensitivity X-Ray Ptychographic Coherent Diffraction Imaging Using the CITIUS Detector," *Journal of Synchrotron Radiation* 30 (2023): 989, https://doi.org/10.1107/S1600577523004897.

65. M. García, M. J. Aguirre, G. Canzi, C. P. Kubiak, M. Ohlbaum, and M. Isaacs, "Electro and Photoelectrochemical Reduction of Carbon Dioxide on Multimetallic Porphyrins/Polyoxotungstate Modified Electrodes," *Electrochimica Acta* 115 (2014): 146, https://doi.org/10.1016/j.electacta.2013.10.142.

66. M. Girardi, S. Blanchard, S. Griveau, et al., "Electro-Assisted Reduction of CO_2 to CO and Formaldehyde by $(TOA)_6[\alpha\text{-}SiW_{11}O_{39}Co(_)]$ Polyoxometalate," *European Journal of Inorganic Chemistry* (2015): 3642, https://doi.org/10.1002/ejic.201500389.

67. S.-X. Guo, D. R. MacFarlane, and J. Zhang, "Bioinspired Electrocatalytic CO_2 Reduction by Bovine Serum Albumin-Capped Silver Nanoclusters Mediated by $[\alpha\text{-}SiW_{12}O_{40}]^{4-}$," *ChemSusChem* 9 (2016): 80, https://doi.org/10.1002/cssc.201501343.

68. S.-X. Guo, F. Li, L. Chen, D. R. MacFarlane, and J. Zhang, "Polyoxometalate-Promoted Electrocatalytic CO_2 Reduction at Nanostructured Silver in Dimethylformamide," *ACS Applied Materials & Interfaces* 10 (2018): 12690, https://doi.org/10.1021/acsami.8b01042.

69. Y.-R. Wang, Q. Huang, C.-T. He, et al., "Oriented Electron Transmission in Polyoxometalate-Metalloporphyrin Organic Framework for Highly Selective Electroreduction of CO_2," *Nature Communications* 9 (2018): 4466, https://doi.org/10.1038/s41467-018-06938-z.

70. M. Girardi, D. Platzer, S. Griveau, et al., "Assessing the Electrocatalytic Properties of the $\{Cp^*Rh^{III}\}^{2+}$-Polyoxometalate Derivative $[H_2PW_{11}O_{39}\{Rh^{III}Cp^*(OH_2)\}]^{3-}$ Towards CO_2 Reduction," *European*

15213765, 2026, 40, Downloaded from https://chemistry-europe.onlinelibrary.wiley.com/doi/10.1002/chem.71437 by Koji Harano - National Institute For , Wiley Online Library on [28/10/2026]. See the Terms and Conditions (https://onlinelibrary.wiley.com/terms-and-conditions) on Wiley Online Library for rules of use; OA articles are governed by the applicable Creative Commons License

Journal of Inorganic Chemistry (2019): 387, https://doi.org/10.1002/ejic.201800454.

71. J. Du, Z.-L. Lang, Y.-Y. Ma, et al., "Polyoxometalate-based Electron Transfer Modulation for Efficient Electrocatalytic Carbon Dioxide Reduction," *Chemical Science* 11 (2020): 3007, https://doi.org/10.1039/C9SC05392A.

72. Y.-J. Liu, P. Shao, M.-Y. Gao, W.-H. Fang, and J. Zhang, "Synthesis of Ag-Doped Polyoxotitanium Nanoclusters for Efficient Electrocatalytic CO_2 Reduction," *Inorganic Chemistry* 59 (2020): 11442, https://doi.org/10.1021/acs.inorgchem.0c01245.

73. C. Li, B. Zha, and J. Li, "A SiW_{11}Mn-Assisted Indium Electrocatalyst for Carbon Dioxide Reduction Into Formate and Acetate," *Journal of CO2 Utilisation* 38 (2020): 299, https://doi.org/10.1016/j.jcou.2020.02.008.

74. D. Zang, Q. Li, G. Dai, M. Zeng, Y. Huang, and Y. Wei, "Interface Engineering of Mo_8/Cu Heterostructures Toward Highly Selective Electrochemical Reduction of Carbon Dioxide Into Acetate," *Applied Catalysis B* 281 (2021): 119426, https://doi.org/10.1016/j.apcatb.2020.119426.

75. H. Yang, D. Yang, Y. Zhou, and X. Wang, "Polyoxometalate Interlayered Zinc–Metallophthalocyanine Molecular Layer Sandwich as Photocoupled Electrocatalytic CO_2 Reduction Catalyst," *Journal of the American Chemical Society* 143 (2021): 13721, https://doi.org/10.1021/jacs.1c05580.

76. J. Ying, B. Zhang, A. Tian, and X. Wang, "A Series of A- and B-type Anderson Compounds With Al, Te and Cr as Centers by Tuning Different Ligands: Syntheses, Electrochemical, Photocatalytic and CO_2RR Properties," *CrystEngComm* 23 (2021): 2572, https://doi.org/10.1039/D1CE00185J.

77. H. Yu, J. Ying, Y. Tian, and A. Tian, "Synthesis, Structure and Properties of a Three-Dimensional Polyoxometalate-Based Compound Modified by Two Organic Ligands," *Inorganic Chemistry Communications* 123 (2021): 108338, https://doi.org/10.1016/j.inoche.2020.108338.

78. B. Zhang, J. Ying, X. Zhang, C. Wang, and A. Tian, "Electrocatalytic, Photocatalytic, Fluorescence Sensing and CO_2RR Properties of a Series of Homopolymolybdate Hybrid Coordination Polymers," *New Journal of Chemistry* 45 (2021): 13340, https://doi.org/10.1039/D1NJ02283K.

79. J. Liu, S. Wang, N. Liu, et al., "Au-Polyoxometalates A-B-A-B Type Copolymer-Analogue Sub-1 Nm Nanowires," *Small* 17 (2021): 2006260, https://doi.org/10.1002/smll.202006260.

80. W. Sun, C. Li, and H. Zhao, "The Targeted Multi-Electrons Transfer for Acetic Acid and Ethanol Obtained With $(n\text{-}Bu_4N)_3SVW_{11}O_{40}$ and in Synergetic Catalysis in CO_2 Electroreduction," *Journal of Power Sources* 517 (2022): 230665, https://doi.org/10.1016/j.jpowsour.2021.230665.

81. Q. Huang, Q. Niu, X.-F. Li, et al., "Demystifying the Roles of Single Metal Site and Cluster in CO_2 Reduction via Light and Electric Dual-Responsive Polyoxometalate-Based Metal-Organic Frameworks," *Science Advances* 8 (2022): eadd5598, https://doi.org/10.1126/sciadv.add5598.

82. S.-Q. Li, L.-F. Dai, Y.-Q. Tian, Y.-X. Yi, J. Yan, and C. Liu, "Polymolybdate-Guided Assembly of a Thiacalix[4]Arene-Protected Ag Nanocluster for Electrocatalytic CO_2 Reduction," *Chemical Communications* 59 (2023): 575, https://doi.org/10.1039/D2CC05692E.

83. M.-T. Peng, C. Chen, Y. Zhang, J.-Y. Xu, Y.-L. Teng, and B.-X. Dong, "Exploring the Role of Sandwich-Type Polyoxometalates in $\{K_{10}(PW_9O_{34})_2M_4(H_2O)_2\}$@PCN-222 (M = Mn, Ni, Zn) for Electroreduction of CO_2 to CO," *Dalton Transactions* 52 (2023): 10737, https://doi.org/10.1039/D3DT01535A.

84. W. Sun, Y. Tai, W. Tian, L. Zhou, and C. Li, "Electrochemical CO_2 Reduction to Ethanol: Synergism of $(n\text{-}Bu_4N)_3SVMo_{11}O_{40}$ and an In Catalyst," *Electrochimica Acta* 445 (2023): 142067, https://doi.org/10.1016/j.electacta.2023.142067.

85. T. Tubul-Sterin, M. Baranov, G. Gan-Or, N. Leffler, A. Neyman, and I. A. Weinstock, "Polyoxometalate-Complexed Indium Hydroxide: Atomically Homogeneous Impregnation via Countercation Exchange," *Inorganic Chemistry* 62 (2023): 1804, https://doi.org/10.1021/acs.inorgchem.1c03857.

86. W. Sun, D. Yao, Y. Tai, et al., "Efficient Electrocatalytic CO_2 Reduction to Ethanol Through the Proton Coupled Electron Transfer Process of $PV_nMo_{(12-n)}$ (n = 1, 2, 3) Over Indium Electrode," *Journal of Colloid & Interface Science* 650 (2023): 121, https://doi.org/10.1016/j.jcis.2023.06.167.

87. W. Sun, L. Zhou, W. Tian, S. Li, M. Yang, and C. Li, "Selective CO_2 to Proportionally Tunable Syngas at Lower Onset Potential Enabled by Bimetallic Chalcogenides in Polyoxometalate Medium," *Applied Catalysis B* 356 (2024): 124206, https://doi.org/10.1016/j.apcatb.2024.124206.

88. L. Shu, C. Li, M.-T. Peng, M.-J. Liu, Y.-L. Teng, and B.-X. Dong, "Heterogenization of a Sandwich $[(PW_9O_{34})_2Co_4(H_2O)_2]^{10-}$ in PCN-222/PCN-222(M): Exploring the Electron Transfer for Electrocatalytic CO_2 Reduction," *European Journal of Inorganic Chemistry* 27 (2024): e202400485, https://doi.org/10.1002/ejic.202400485.

89. Y. Zhang, C. Li, L. Shu, Y.-L. Teng, and B.-X. Dong, "Research on the Construction of a Series of Transition Metal-Substituted Keggin-Type TMSPOMs@PCN-224 Composites Through the Encapsulation Method and Their Electron Transfer Mechanism in CO_2RR," *Inorganic Chemistry* 63 (2024): 11592, https://doi.org/10.1021/acs.inorgchem.4c00840.

90. J.-J. Liang, Y.-C. Zhang, Z.-H. Chang, et al., "Two New 6-nitrobenzimidazole Ligand-Modified Polymolybdate-Based Metal–Organic Complexes With Excellent Capacitive and Electrocatalytic Performances," *New Journal of Chemistry* 48 (2024): 1248, https://doi.org/10.1039/D3NJ04841A.

91. Y. Tai, W. Sun, D. Yao, et al., "Keggin-Type P-W-Mo-V Polyoxometalates in Electrocatalyzed CO_2 Reduction Using Indium Electrodes," *Polyoxometalates* 3 (2024): 9140051, https://doi.org/10.26599/POM.2023.9140051.

92. P. Zhang, W.-X. Shi, H.-Q. Yin, et al., "W_{10} Single-Cluster-Mediated Syngas Electrosynthesis in Single-Sandwich-Layer ZnAl-Layered Double Hydroxide Catalysts," *ACS Nano* 19 (2025): 37206, https://doi.org/10.1021/acsnano.5c11814.

93. C. Liu, L. Song, W. Wu, H. Li, D. Dang, and Y. Bai, "Photo-coupled Electrocatalytic Conversion of CO_2 to CO Over Cobalt Phthalocyanine-Modified POM-$K_8Ta_6O_{19}$ Z-Scheme Photocathodes," *Green Chemistry* 27 (2025): 15607, https://doi.org/10.1039/D5GC04093K.

94. W. Sun, C. Li, Y. Tai, L. Zhou, W. Tian, and S. Li, "Selective Proton-Coupled Electron Transfer Engineering Between Cu_xIn_y Alloy and Polyoxometalate Medium for Efficient CO_2 Electroreduction to CO," *Journal of Catalysis* 450 (2025): 116254, https://doi.org/10.1016/j.jcat.2025.116254.

95. W. Sun, C. Li, L. Zhou, W. Tian, S. Li, and M. Yang, "Engineering the Interface Charge Redistribution and Boosted Kinetics via Polyoxometalate for Efficient Carbon Dioxide Electroreduction in Acidic Medium," *Journal of Colloid & Interface Science* 697 (2025): 137912, https://doi.org/10.1016/j.jcis.2025.137912.

96. K. Xia, T. Yatabe, K. Yonesato, et al., "Structural Engineering of Au—Ag Heterometallic Nanoparticles Using Multidentate Polyoxometalate Ligands," *Small* 22 (2026): e14728, https://doi.org/10.1002/smll.202514728.

Supporting Information

Additional supporting information can be found online in the Supporting Information section.

Supporting File 1: chem71437-sup-0001-SuppMat.pdf The authors have cited additional references within the Supporting Information [60–96]. The Supporting Information includes experimental section and supplementary figures and tables.

15213765, 2026, 40, Downloaded from https://chemistry-europe.onlinelibrary.wiley.com/doi/10.1002/chem.71437 by Koji Harano - National Institute For , Wiley Online Library on [28/10/2026]. See the Terms and Conditions (https://onlinelibrary.wiley.com/terms-and-conditions) on Wiley Online Library for rules of use; OA articles are governed by the applicable Creative Commons License